Electrodynamics and energy characteristics of aurora at high resolution by optical methods

H. Dahlgren,[1,2] B. S. Lanchester,[2] N. Ivchenko,[1] D. K. Whiter[2]

Corresponding author: H. Dahlgren, Space Environment Physics, University of Southampton, Southampton SO17 1BJ, UK. (hannad@kth.se)

[1]Space Plasma Physics, Royal Institute of Technology, Stockholm, Sweden

[2]Space Environment Physics, University of Southampton Southampton, UK

Key Points.

- High resolution multi-spectral imaging is used to study the nature and source of dynamic aurora.
- A new optical method is presented to investigate ionospheric electrodynamics by tracing plasma flows.
- The ASK instrument also gives estimates of auroral energy and flux at unprecedented resolution.

Abstract. Technological advances leading to improved sensitivity of optical detectors have revealed that aurora contains a richness of dynamic and thin filamentary structures, but the source of the structured emissions is not fully understood. In addition, high resolution radar data have indicated that thin auroral arcs can be correlated with highly varying and large electric fields, but the detailed picture of the electrodynamics of auroral filaments is yet incomplete. The ASK instrument is a state-of-the-art ground-based instrument designed to investigate these smallest auroral features at very high spatial and temporal resolution, by using three EMCCDs in parallel for three different narrow spectral regions. ASK is specifically designed to utilize a new optical techique to determine the ionospheric electric fields. By imaging the long-lived O^+ line at 732 nm, the plasma flow in the region can be traced, and since the plasma motion is controlled by the electric field, the field strength and direction can be estimated at unprecedented resolution. The method is a powerful tool to investigate the detailed electrodynamics and current systems around the thin auroral filaments. The two other ASK cameras provide information on the precipitation by imaging prompt emissions, and the

emission brightness ratio of the two emissions, together with ion chemistry modeling, is used to give information on the energy and energy flux of the precipitating electrons. In this paper, we discuss these measuring techniques, and give a few examples of how they are used to reveal the nature and source of fine scale structuring in the aurora.

1. Introduction

Advances in imaging technology have in the last decades enriched the field of auroral science with observations of extremely rapid variations and thin filaments in auroral displays. A large data base of observations with scale sizes of less than 100 m and temporal variations of milliseconds has been collected, which in turn has led to the development of more advanced methods to study the characteristics of the structures, to classify them and to understand their origin. The processes behind the structuring of aurora into thin filaments as narrow as 100 m perpendicular to the geomagnetic field is not yet fully understood. Pioneering work investigated the occurrence of fine scale widths and distortions such as auroral curls from high-resolution television data [e.g. Maggs and Davis, 1968; Trondsen and Cogger, 1998, 2001]. Recent efforts have been devoted to high-speed imaging ($>$ 100 frames per second) of rapid variations in the aurora, such as flickering and pulsations [e.g. Kataoka et al., 2011; Yaegashi et al., 2011; Nishiyama et al., 2014].

A better understanding of the role of electric fields in the electrodynamics in the ionosphere, and its coupling to the magnetosphere, is essential to find the source of the dynamics of auroral filaments and what causes the fast spatial structuring. Highly structured auroral precipitation can lead to ionospheric feedback mechanisms as a result of strong conductivity gradients and formation of small-scale currents and waves; the ionosphere can thus act as a generator which drives auroral dynamics [e.g. Lu et al., 2008; Russell et al., 2013]. Extremely large and short-lived electric fields of several hundred mV/m have been discovered by high-resolution measurements in the ionosphere adjacent to bright auroral arcs [Lanchester et al., 1996]. Such strong fields have important implications for the

energy deposition in the ionosphere through Joule heating. Ionospheric electric fields can be measured directly in situ by rockets and satellites, or indirectly, by measuring plasma motion induced by the electric fields, with Doppler shift observations from coherent and incoherent scatter radars or Fabry-Perot interferometers. These methods are limited mainly by their low spatial resolution when trying to investigate the electrodynamics of fine scale aurora. To understand the structured current closure and feedback processes which make up the ionospheric electrodynamic system, high resolution measurements of the electric field are crucial to probe the smallest scales and fastest dynamics, in order to include the measurements in current theories. Here we discuss a newly developed technique to use optical traces of plasma flows in the ionosphere at very high spatial (0.012°) and temporal (0.031 s) resolution to estimate the local electric field strength and direction adjacent to auroral arcs.

Multi-spectral imaging of the aurora provides information about the incident electron spectrum, since emissions from different species are dependent on the energy of the precipitating electrons. The common approach is to measure the emission ratio between two emissions sensitive to low and high energy electrons respectively, and compare this ratio with those predicted by electron transport and ion chemistry models. Using high resolution optical instruments and incoherent scatter radar, Lanchester et al. [1997] noted a very large energy flux (>500 mW/m^2) within a 100-m wide filament of mono-energetic precipitation, located within a wider region of precipitation of lower energy flux. Other observations of auroral filaments and curls have shown that they are associated with both higher energy and higher electron fluxes than the surrounding precipitation [Lanchester et al., 2009; Dahlgren et al., 2008b, 2012]. Ivchenko et al. [2005] showed that curls are

caused by high energy precipitation, which would be a signature of an electrostatic acceleration mechanism above the ionosphere, whereas auroral rays are the result of both high and low energy electrons, which indicates acceleration by wave-particle interactions. Thus, identifying the characteristics of the electron spectra provides important information on what electron acceleration mechanisms are acting above the ionosphere.

2. The challenges in measuring the spatial and temporal variations of fine-scale aurora

Ground-based measurements are currently required to resolve the finest dynamics of auroral structures, and are also the easiest and cheapest to conduct. The same region of the sky can be monitored for hours at high temporal resolution, compared with measurements from a satellite or rocket which moves at several km per second. The biggest difficulty in imaging the optical aurora is obtaining measurements with simultaneous high spatial, temporal and spectral resolution, with sufficient signal-to-noise ratio. The invention of electron multiplying CCDs (EMCCDs) provided a great leap forward in high resolution imaging of low photon auroral events, compared with TV cameras and conventional CCD detectors. The photoelectrons that are generated in the silicon on the CCD chip are multiplied through impact ionization by a solid state electron multiplying register, before any readout noise is added by the output amplifier. As a result, even single photon events can be amplified above the read noise floor. However, the high gain constrains the dynamic range of the measurements, especially if the pixel size is relatively small. In addition, just as for intensified CCDs (ICCDs), there will be an additional multiplicative noise caused by the gain register, which can be accounted for by increasing the shot noise by a factor of $\sqrt{2}$.

The scientific-grade CMOS (sCMOS) detector uses a recently developed technology which is also capable of providing high resolution observations and low noise without the addition of multiplicative noise, and at a lower cost. Each pixel is composed of a photodiode and an amplifier, so that the signal is multiplied at each pixel as the charge is converted to voltage. The larger CMOS chip has smaller pixels than an EMCCD chip, which leads to potentially increased spatial resolution at higher temporal resolution. However, for extreme low-light conditions, which is often the case for narrow-band spectral observations of fine-scale aurora, the EMCCD will outperform the sCMOS, with higher signal-to-noise ratio [Joubert and Sharma, 2011].

When using emission ratio measurements to infer the electron spectrum of the auroral precipitation, particular attention must be paid to the viewing geometry of the imager. The emissions are distributed in height along the geomagnetic field lines and the measured brightness for each emission is the integrated intensity along the line of sight of the imager. The same emissions are modeled by assuming a range of input spectra for the precipitating electrons. These emissions are integrated along the magnetic field direction. The ratios of the measured and modeled emissions can then be compared in order to estimate the energy of the precipitation. Therefore it is essential that the imager is aligned with the field so that the aurora is viewed in the magnetic zenith. The viewing geometry is also important for estimating the scale sizes of filamentary aurora. In Figure 1 the two images show an auroral filament separated by 0.7 s, captured with an imager with a field-of-view (FOV) of $3^\circ \times 3^\circ$. In the left image, as the structure passes through magnetic zenith (marked with a white square), its width is 80 m (estimated as the full-width-at-half-maximum of a fitted Gaussian to its profile perpendicular to the geomagnetic field and assuming an

auroral altitude of 100 km), whereas in the right image, where the structure has moved approximately 1 km from magnetic zenith, the same estimate results in an ambiguous width of 600 m. In addition, the exposure time needs to be short enough to avoid smearing due to any motion of the aurora. For a detailed discussion on viewing geometry of aurora, see Romick and Belon [1967]. To expand emission-ratio techniques to regions outside the zenith, careful modeling or assumptions must be introduced. Tuttle et al. [2014] recently demonstrated a powerful method to estimate the auroral electron energy spectra in a region of a few degrees surrounding the magnetic zenith by reconstructing auroral 2-D images from modeled 3-D emission rates, where the emission rates were based on look-up tables of correlated radar and optical data. The similarity between the reconstructed images and auroral observations demonstrated the strength of the method to estimate the volume emission rates also in a region outside the magnetic zenith.

3. The ASK instrument

The Auroral Structure and Kinetics (ASK) instrument was developed to investigate the physics behind the finest structures in the aurora, by multi-monochromatic imaging of aurora in magnetic zenith at very high spatial and temporal resolution. The instrument consists of three co-aligned imagers and two photometers, each equipped with a narrow-band interference filter to monitor different parts of the auroral spectrum simultaneously. The detector on each imager is an EMCCD with 512 $\times$ 512 pixels. The chip is binned 2 $\times$ 2, which allows for faster readout speeds. The cameras are connected to the same electronics unit, through which they get their triggering pulses. Time synchronization on all three channels is ensured by the input of a 1 pulse-per-second signal from a GPS. Images are captured at 20 Hz during regular observation mode, and 32 Hz for special mode, during

radar runs or other events. The cameras are equipped with F/1 lenses with a focal length of 75 mm, providing a FOV of 6.2° × 6.2°, corresponding to 10 km × 10 km at auroral altitudes. Galilean-type converters with a 2 × angular magnification can be fitted to the system, resulting in a FOV of 3.1° × 3.1°. The system is automatically switched on and off by the signal of a light sensor, and every 20 min the data acquisition is paused for 20 s and the shutter closed, to take dark frames. At maximum frame rate (32 Hz), each of the three cameras produces more than 14 GB/hour of data. Overview stackplots of vertical slices through the images as a function of time, so called keograms, are automatically created, and every few days the keograms are inspected to delete any high resolution data where no aurora was detected. 2-s mean images are saved for all periods. The data is then written to 800 GB LTO-4 Ultrium tapes. At its fastest run mode, ASK has a temporal resolution of 0.031 s and spatial resolution of 0.012° (approximately 20 m at 100 km altitude). The images are absolute intensity calibrated each season using the tabulated spectral flux of stars from the Pickles star catalogue [Pickles, 1998].

ASK was initially deployed at the EISCAT Svalbard Radar (ESR) at 78°N in 2005. It was moved to the Norwegian mainland and run from the EISCAT site outside Tromsø (69°N) during the winter 2006-2007, after which it was moved back to Svalbard, and is currently operating there around the clock during the polar winter.

4. Technique to estimate electric fields from optical measurements of O^+ flow

Optical measurements of a forbidden oxygen ion multiplet in the ionosphere provide a unique opportunity to derive estimates of the local electric field and its variability at high resolution. One of the ASK imagers is equipped with a narrowband (full width at half maximum of 1.0 nm) transmission filter centered at 732.0 nm, for observations of

the forbidden oxygen emissions which originate from the O^+ ^2P state. The filter almost completely excludes the 733 nm emissions originating from the same state, as the filter transmission is 5.5% at 733 nm. Due to the relatively long life time of this excited state – up to 5 s in the ionospheric F region - it is possible to trace the flow of the plasma from the motion of the resulting auroral emissions as the ions de-excite to a lower state. Since the collision frequency with neutrals at this altitude is negligible, the plasma motion is governed by the local $\mathbf{E} \times \mathbf{B}$-drift, so that tracing the plasma motion provides an estimate of the magnitude and direction of the local electric field.

4.1. Chemistry of the forbidden O^+ emission doublet at 732/733 nm

The metastable O^+ ^2P state is mainly produced in the ionospheric F region, at typical altitudes of 200 - 350 km, through excitation of oxygen atoms by soft precipitation of primary and secondary electrons through

$$e + O \rightarrow 2e + O^+(^4S, ^2P, ^2D), \tag{1}$$

where approximately 18% of the ionization results in the ^2P state [Rees et. al., 1982]. This state is divided into two levels with different total angular momentum: $^2P_{1/2}$ and $^2P_{3/2}$. The losses consist of both emissions as well as quenching (de-excitation by collisions), so that the density n of the state is governed by

$$\frac{dn}{dt} = \eta - \sum_i A_i n - \sum_k \alpha_k n(X_k) n. \tag{2}$$

Here η is the production rate, the second term on the right is the radiation loss term, A_i is the Einstein transition probability for the ith emission, and the third term is losses due to quenching by species X_k where α_k is the corresponding quenching rate coefficient. Four transitions from the $^2P_{1/2,3/2}$ states to the $^2D_{3/2,5/2}$ states produce two auroral doublet

emissions in the near infrared, at 732.0 nm and 733.0 nm [Vallance Jones, 1974; Rees et. al., 1982]. The effective lifetime, τ, of the ^{2}P state is height dependent, due to the quenching, so that lower energies give a longer decay time and brighter O^+ emissions. The theoretical lifetime increases from about 1 s at 200 km altitude to 5 s at above 350 km altitude. The emissions are further described in Dahlgren et al. [2008a, 2009].

The relative brightness of the 732.0 nm and 733.0 nm emissions depend on the relative population of the two ^{2}P states, which was recently investigated in detail by Whiter et al. [2014], who found that the brightness ratio in aurora will depend on the neutral temperature in the ionosphere. The discovery opens up the opportunity for a new spectral method to estimate the neutral temperatures and its variations in the auroral region.

4.2. N_2 1PG contamination

The O^+ lines at 732 nm and 733 nm are not the only emissions in this part of the auroral spectrum. Band emission from N_2 1PG (6,4) and (5,3) and the (8,3) Meinel band of OH airglow contaminate the ASK measurements in this spectral region, and for a quantitative analysis of the O^+ ^{2}P emission these need to be removed. In their analysis of O^+ measurements, Semeter et al. [2001] used simultaneous imaging of the N_2^+ 1N (0,1) band at 427.8 nm as a proxy for the N_2 1PG contribution, since this emission originates from the same parent N_2 population. The amount of contamination is highly dependent on the energy and energy flux of the precipitating electrons. The N_2 emissions peak in the E region, at about 110 km, whereas the O^+ emissions are from above 200 km. In a later work, Semeter et al. [2003] distinguished between the emissions using the oblique (to the background geomagnetic field) viewing geometry of multispectral allsky images to investigate the height separation of the emissions. Dahlgren et al. [2008a] characterized

the different contaminating species for different electron energy spectra, using individual reference spectra of the various contaminating emissions obtained from high resolution spectrographic measurements, and weighting these to produce the total measured spectrum. That way, the different contributions of the various contaminating species could be determined for each time step.

A different method to estimate the contamination of the O^+ emissions was presented by Spry et al. [2014], based on imager data from ASK in combination with modeled synthetic spectra of the N_2 1PG (5,3) emission band. Unlike the methods described above, variations of the rotational and vibrational temperature of molecular nitrogen can now be taken into account. The 673 nm filter on ASK provides information on the contribution of N_2 1PG (5,3) through

$$B_{(5,3)} = B_{673} \times \left(\frac{I_{732}}{I_{673}}\right)_{mod} \tag{3}$$

where $(I_{732}/I_{673})_{mod}$ is the temperature-dependent modeled transmission ratio of the N_2 1PG (5,3) band emission at 732 nm and the N_2 1PG (5,2), (4,1) and (3,0) band emissions at 673 nm, and B_{673} is the measured brightness from ASK. The modeled transmission ratio is derived from synthetic N_2 spectra. More information on this method to remove the contamination from the O^+ data is given in Spry et al. [2014] and references therein. For any such detailed spectral analysis it is important to keep the filter temperature constant, as the transmission curve is temperature dependent.

4.3. Deriving the electric field

Once the ASK O^+ emissions are cleaned from contamination, they can be used to trace the motion of the F-region plasma. At these altitudes the plasma flow can be assumed

to be governed by the local electric field and perpendicular to the field direction, with $|E| = |v| \cdot |B|$, where the geomagnetic field strength B is obtained from the IGRF model. Emissions detected in the other ASK channels provide information on the prompt emissions, which are used to separate the motion of the source from that of the plasma flows in the region. The variability of the electric field can therefore be determined at high temporal resolution. Examples of events when the technique has been demonstrated are given in Section 6.1.

5. Estimation of energy and energy flux

The method of using different emission ratios to estimate the energy of the auroral precipitation has a long history, with different emissions and different ionospheric models used in the analysis [e.g. Rees and Luckey, 1974; Strickland et al., 1989; Meier et al., 1989; Hecht et al., 1989; Gustavsson et al., 2001; Semeter et al., 2001]. For energy analysis of fine scale aurora, observations of prompt emissions are necessary to monitor the rapid changes in the precipitation. The high energy precipitation is monitored in ASK using either a filter for observations of O_2^+ 1N (first negative) emissions at 562.0 nm or N_2 1PG (first positive) emissions at 673.0 nm. Another ASK channel monitors the prompt emissions from the atomic oxygen line at 777.4 nm, produced by electron impact excitation of O in the F region. With an excitation threshold just above 10 eV, this emission is a good measure of low energy precipitation. However, the 777.4 nm emission can also be created in a dissociative process by electron impact on O_2, so that it has a contribution from higher energy precipitation. The emission is further described in Lanchester et al. [2009]. The ratio of measured brightness in the high energy channel and the 777.4 nm channel are then compared with modeled ratios, using the Southampton ion chemistry and electron

transport model [Lanchester et al., 1994, 1997]. Modeled brightnesses through the filters on ASK as a function of energy of the precipitating electrons, produced with a Gaussian-shaped input spectrum with a constant flux of 1 mW/m^2, can be found in Figure 3 in Whiter et al. [2010]. A modeled ratio derived for each specific event is compared with measured ratios from the ASK instrument to estimate the energy. Since both the O_2^+ emission brightness at 562 nm and the N_2 emission brightness at 673 nm are close to constant for energies above 1 keV, these emissions can be used as a proxy for the energy flux. Uncertainties in using emission ratios to estimate the energy of the precipitation are mainly due to variations in the atmospheric neutral composition, horizontal drifts, uncertainties in the measurements and in the emission cross sections. For a more thorough description and discussion of this method to estimate the energy spectrum, the reader is referred to Lanchester and Gustavsson [2012].

6. Novel scientific results from ASK

This section gives some brief examples of how the optical techniques based on ASK data have been used to investigate the electrodynamics and energy characteristics correlated with fine scale aurora, to better understand its source and formation.

6.1. Electric fields from optical plasma flows

The technique to estimate ionospheric electric fields by tracing afterglowing plasma has been demonstrated on a few events using data from ASK [Dahlgren et al., 2009]. One O^+ afterglow event from 9 Nov 2006 is shown in Figure 2. Here, the motion of the afterglowing plasma blob is traced by calculating the cross-correlation between the region of interest containing the full structure and same-sized regions in the ASK FOV in

subsequent frames of the O^+ channel. Figure 2 a) shows the initial O^+ image (without contamination removal) with the selected region of interest marked with a white box. At this time, the feature can also be seen in the prompt emissions. Figure 2 b) is the O^+ image 2.5 s later. The brightness of the auroral feature has decayed though it is still visible. The black '+' markers show the trace of the center of the region of interest with highest cross correlation, with the black box indicating the most recent region. The red box signifies the turn-off point, where the prompt emission ceases, leaving only the afterglow measured in the O^+ channel. The prompt emissions at these two instances of time are shown in Figure 2 c) and d), where the traced feature can only be seen in c). There is a slight shift in the direction of the moving feature, with a stronger northward component during the first second of the interval. The structure is also slowing down somewhat, from an initial speed of 850 m/s to 600 m/s (at an emission height of 250 km), which corresponds to electric field strengths of 40 mV/m and 29 mV/m, respectively. The electric field estimate scales with the height of the O^+ emission, which is estimated by comparing the decay time of the emission with modeled decay times for different heights, as shown in Dahlgren et al. [2009].

These results demonstrate the powerful capability to use the O^+ afterglowing emissions to estimate electric fields at very high spatial and temporal resolution. A limitation to the method is that the electric field can only be estimated in regions where O^+ emissions are present. For a better understanding of the spatial distribution of electric fields, more sophisticated tracing algorithms should be implemented, such as optical flow reconstruction methods, to estimate a full 2-D flow field in the region and confidently carry out time-dependent analysis of electric fields associated with active aurora.

6.2. Energy and energy flux of dynamic aurora

The method to estimate energy and energy flux from observations and modelling as outlined in section 3 has been applied to several ASK data sets. Lanchester et al. [2009] demonstrated the strength of the method by determining the peak energy and flux of the precipitation forming a number of dynamic auroral events with widths of the order of 100 m perpendicular to the geomagnetic field. Dahlgren et al. [2011] used the technique in an investigation of the role of sheared aurora at boundary regions. In the study, it was found that a thin, sheared auroral arc appeared on the boundary between two different precipitating electron populations of different energies, where an energy gradient and increased number flux were present. The increased electron flux was likely produced by Alfvén waves that were launched above the ionosphere in the boundary region, with associated large and variable electric fields causing the shear flow.

The detailed multi-spectral imaging capability of ASK has recently led to the intriguing discovery that auroral structures caused by either high or low energy precipitation can co-exist and overlap in the ionosphere as they move in different directions, with different apparent speeds [Dahlgren et al., 2015]. Figure 3, top row, shows three snapshots from the ASK cameras, taken on 15 Dec 2006, where the emissions from the O_2^+ channel (emissions sensitive to high energy precipitation) are displayed in red scale and the emissions from O^+ (emissions sensitive to low energy precipitation) are in green scale. For the low energy precipitation in this event, data from the O^+ channel are shown rather than data from the O channel, due to a higher signal-to-noise ratio. The individual images from the two channels are shown below each snapshot, and a video of the event can be downloaded from the auxiliary material. An auroral structure (red) with a sharp edge, caused by high

energy precipitation, is seen to move to the left in the image sequences. The outline of the edge and the direction of motion is marked in gray in the middle panel. At the same time, an oval-shaped auroral feature caused by low energy precipitation (green, and outlined in black in the middle panel), is overlapping the edge, and only slowly drifting upwards in the images. Careful analysis of the event showed that the apparent overlap of the structures is not just a perspective effect due to the emissions originating from different heights, and the structures do not interact as they cross on the same geomagnetic field lines. It is suggested that two different acceleration mechanisms are acting simultaneously on the same field lines, but at different distances from earth. A possible scenario is that the high energy electrons were accelerated in the auroral acceleration region and then structured into thin filaments by local instabilities above the ionosphere, whereas the low energy electrons may be the result of wave-particle interactions with oblique Alfvén waves just above the ionosphere.

Another event study from the same night revealed extremely thin auroral filaments of less than 100 m widths caused by precipitation of 8 keV electrons during a substorm breakup. No energy dispersion signatures were found in the data and the lack of perspective effects when monitoring the thin structures away from magnetic zenith indicated that the energy distribution of the precipitation was sharply peaked, with an energy flux of 230 mW/m^2. This is at odds with the electrons being accelerated by Alfvén waves, and the flux is larger than that usually observed for inverted-V precipitation. The thin structures were embedded in a broader region of less structured aurora of lower energy (about 4 keV). Details of the event and analysis can be found in Dahlgren et al. [2012]. It is not yet clear what formation mechanism could cause such thin, mono-energetic struc-

315 tures, but a possibility of the source of the structuring into thin filaments is that different
316 instabilities grow on the impinging current sheets from the magnetosphere [e.g. Seyler,
317 1990; Otto and Birk, 1993; Chaston and Seki, 2010].

7. Summary

318 In this paper we discuss two measurement techniques to use multi-spectral optical data
319 at very high temporal and spatial resolution, captured with the ASK instrument, to inves-
320 tigate the nature and source of dynamic aurora by studying the detailed electrodynamics
321 and energy spectra of the precipitation. The first is a new technique to estimate the elec-
322 tric fields in the ionosphere and its evolution by tracing the optical flow of O^+ emissions.
323 The emission is produced by low energy electron precipitation and due to the lifetime of
324 approximately 5 s of the excited state, the motion of the plasma can be traced after the
325 precipitation has ceased. In the collisionless plasma at these altitudes, the plasma motion
326 is governed by the local electric field. The spectral region around the oxygen emission
327 includes emission bands of other species, and the emissions must be carefully separated
328 to distinguish the afterglowing oxygen from prompt emissions or airglow. Initial results
329 of the technique show promise of a powerful method to investigate the temporal evolu-
330 tion of the electric field at high resolution. Further development of flow algorithms and
331 modeling of the 2-D response taking the height-variability of the decay into account will
332 provide information on the spatial distribution of the electric field surrounding auroral
333 arc filaments, which will be of importance for studies of the dynamics of fine scale aurora.
334 The second technique discussed in this paper is the use of multi-spectral imaging to-
335 gether with modeling to estimate the energy spectrum of the precipitating electrons caus-
336 ing the auroral emissions, and its evolution over time. The multi-spectral ASK data

have shown that filamentary aurora can form due to an increase of particle flux on the boundary between two electron populations of different energies. Fine scale aurora can also be produced by mono-energetic precipitation of high energy, and auroral structures produced by electron precipitation of either high or low energy can co-exist with separate morphology and motion pattern. Such information is crucial to understand the formation mechanisms of the finest structures in the aurora.

Acknowledgments. ASK has been funded by PPARC, NERC and STFC of the United Kingdom, and the Swedish research council. HD is supported by the Swedish Research Council under grant 350-2012-6591. For the data used in the research, we thank the EISCAT and ASK campaign teams for running the instruments during several winter campaigns. Requests for data used in this paper can be directed to Hanna Dahlgren (hannad@kth.se).

References

Chaston, C. C., and K. Seki (2010), Small–scale auroral current sheet structuring, *J. Geophys. Res., 115*, A11221, doi:10.1029/2010JA015536.

Dahlgren, H., N. Ivchenko, B. Lanchester, J. Sullivan, D. Whiter, G. Marklund, and A. Stromme (2008a), Using spectral characteristics to interpret auroral imaging in the 731.9 nm O^+ line,*Ann. Geophys., 26*, 10951917, doi:10.5194/angeo-26-1041-2008.

Dahlgren, H., N. Ivchenko, J. Sullivan, B. S. Lanchester, G. Marklund, and D. Whiter (2008b), Morphology and dynamics of aurora at fine scale: first results from the ASK instrument, *Ann. Geophys., 26*, 10411048, doi:10.5194/angeo-26-1041-2008.

Dahlgren, H., N. Ivchenko, B. Lanchester, M. Ashrafi, D. Whiter, G. Marklund, and J. Sullivan (2009), First direction optical observations of plasma flows using afterglow of O^+ in discrete aurora,*J. Atmos. Sol. Terr. Phys., 71*, 228-238.

Dahlgren, H., B. Gustavsson, B. S. Lanchester, N. Ivchenko, U. Brändström, D. Whiter, T. Sergienko, I. Sandahl, and G. Marklund (2011), Energy and flux variations across thin auroral arcs, *Ann. Geophys., 29*, 1–4, doi:10.5194/angeo-29-1-2011.

Dahlgren, H., N. Ivchenko, and B. S. Lanchester (2012), Monoenergetic high-energy electron precipitation in thin auroral filaments, *Geophys. Res. Lett., 39*, L20101, doi:10.1029/2012GL053466.

Dahlgren, H., Lanchester, B. S. and Ivchenko, N. (2015), Coexisting structures from high- and low-energy precipitation in fine-scale aurora, *Geophys. Res. Lett., 42: 1290-1296*, doi: 10.1002/2015GL063173.

Gustavsson, B., Å. Steen, T. Sergienko, B. U. E. Brändström (2001), Estimate of auroral electron spectra, the power of ground-based multi-station optical measurements, *Phys. Chem. Earth, 26*, 189–194, doi:10.1016/S1464-1917(00)00106-9.

Hecht, J. H., A. B. Christensen, D. J. Strickland, and R. R. Meier (1989), Deducing composition and incident electron spectra from ground-based auroral optical measurements: Variation in oxygen density, *J. Geophys. Res., 94*, 13 553–13 563.

Ivchenko, N., E. M. Blixt, and B. S. Lanchester (2005), Multispectral observations of auroral rays and curls, *Geophys. Res. Lett., 32*, L18106, doi:10.1029/2005GL022650.

Joubert, J. R. and D. K. Sharma (2011), EMCCD vs. sCMOS for microscopic imaging, *Photonics spectra, 45(3)*, p. 46–50.

Kataoka R., Y. Miyoshi, T. Sakanoi, A. Yaegashi, Y. Ebihara, K. Shiokawa (2011), Ground-based multispectral high-speed imaging of flickering aurora. *Geophys. Res. Lett., 38*, L14106, doi:10.1029/2011GL048317.

Lanchester, B. S., J. .R Palmer, M. H. Rees, D. Lummerzheim, K. Kaila, and T. Turunen (1994), Energy flux and characteristic energy of an elemental auroral structure, *Geophys. Res. Lett., 21*, 2789-2792.

Lanchester, B. S., K. Kaila, and I. W. McCrea (1996), Relationship between large horizontal electric fields and auroral arc elements, *J. Geophys. Res., 101*, 5075–5084, doi:10.1029/95JA02055.

Lanchester, B. S., M. H. Rees, D. Lummerzheim, A. Otto, H. U. Frey and K. U. Kaila (1997), Large fluxes of auroral electrons in filaments of 100 m width, *Geophys. Res. Lett., 102*, 9741–9748.

Lanchester, B. S., M. Ashrafi, N. Ivchenko (2009), Simultaneous imaging of aurora on small scale in OI (777.4 nm) and $N_2$1P to estimate energy and flux of precipitation, *Ann. Geophys., 27*, 2881–2891.

Lanchester, B. S. and B. Gustavsson (2012), Imaging of aurora to estimate the energy and flux of electron precipitation, *Auroral Phenomenology and Magnetospheric Processes: Earth and Other Planets (eds A. Keiling, E. Donovan, F. Bagenal and T. Karlsson)*, American Geophysical Union, Washington, D. C., doi:10.1029/2011GM001161.

Lu, J. Y., W. Wang, R. Rankin, R. Marchand, J. Lei, S. C. Solomon, I. J. Rae, J.-S. Wang, and G.-M. Le (2008), Electromagnetic waves generated by ionospheric feedback instability, *J. Geophys. Res., 113, A05206*, doi:10.1029/2007JA012659.

401 Maggs, J. E. and T. N. Davis (1968), Measurements of the thicknesses of auroral struc-
402 tures, *Planet. Space Sci., 16*, 205–209.

403 Meier, R. R., D. J. Strickland, J. H. Hecht, and A. B. Christensen (1989), Deducing com-
404 position and incident electron spectra from ground-based auroral optical measurements:
405 A study of auroral red line processes, *J. Geophys. Res., 94*, 13 541–13 552.

406 Nishiyama T., T. Sakanoi, Y. Miyoshi, D. Hampton, Y. Katoh, R. Kataoka, S. Okano
407 (2014), Multi-scale temporal variations of pulsating auroras: on-off pulsation and a
408 few-Hz modulation, *J. Geophys. Res., 119*, doi:10.1002/2014JA019818.

409 Otto, A. and G. T. Birk (1993), Formation of thin auroral arcs by current striation,
410 *Geophys. Res. Lett., 20*,2833–2836.

411 Pickles A. J. (1998), A Stellar Spectral Flux Library: 1150-25000 Å, *Publications of the*
412 *Astronomical Society of the Pacific, 110*, No. 749, 863–878.

413 Rees, M. H., and D. Luckey (1974), Auroral electron energy derived from ratio of spec-
414 troscopic emissions 1. Model computations, *J. Geophys. Res., 79(34)*, 5181-5186.

415 Rees, M. H., V. J. Abreu, and P. B. Hays (1982), The production efficiency of O+(2P)
416 ions by auroral electron impact ionization, *J. Geophys. Res., 87(A5)*, 3612-3616.

417 Romick, G. J., and Belon, A. E. (1967) The spatial variation of auroral luminosity I,
418 *Planetary and Space Science, 15, 3*, 475-493, ISSN 0032-0633.

419 Russell, A. J. B., A. N. Wright, and A. V. Streltsov (2013), Production of small-scale Alfvn
420 waves by ionospheric depletion, nonlinear magnetosphere-ionosphere coupling and phase
421 mixing, *J. Geophys. Res., 118, 1450-1460*, doi:10.1002/jgra.50168.

422 Semeter, J., J. Vogt, and G. Haerendel (2001), Persistent quasiperiodic precipitation of
423 suprathermal ambient electrons in decaying auroral arcs, *J. Geophys. Res., 106*, 12 863–

12 873, doi:10.1029/2000JA000136.

Semeter, J. (2003), Critical comparison of OII(732-733 nm), OI(630 nm), and N_2(1PG) emissions in auroral rays, *Geophys. Res. Lett., 30, 1225*, doi:10.1029/2002GL015828, 5.

Seyler, C. E. (1990), A mathematical model of the structure and evolution of small-scale discrete auroral arcs, *J. Geophys. Res., 95*, 95, 17,199.

Spry, J. D., O. Jokiaho, B. S. Lanchester, D. K. Whiter (2014), Modelling $N_2$1P contamination in auroral O+ emissions, *J. Atmos. Sol. Terr. Phys., 107*, 8–11, ISSN 1364—6826, http://dx.doi.org/10.1016/j.jastp.2013.10.013.

Strickland, D. J., R. R. Meier, J. H. Hecht, and A. B. Christensen (1989), Deducing composition and incident electron spectra from ground-based auroral optical measurements. I - Theory and model results. II - A study of auroral red line processes. III - Variations in oxygen density, *J. Geophys. Res., 94*, 13 527–13 539.

Trondsen, T. S., and L. L. Cogger (1998), A survey of small-scale spatially periodic distortions of auroral forms, *J. Geophys. Res., 103*, 9405 - 9416.

Trondsen, T. S., and L. L. Cogger (2001), Fine-scale optical observations of aurora, *Phys. Chem. Earth (C), 26*, 1–3, 179 - 188.

Tuttle, S., B. Gustavsson, and B. Lanchester (2014), Temporal and spatial evolution of auroral electron energy spectra in a region surrounding the magnetic zenith, *J. Geophys. Res. Space Physics, 119*, doi:10.1002/2013JA019627.

Vallance Jones, A. (1974), Aurora (Geophysics and Astrophysics Monographs), Reidel, Dordrecht.

Whiter, D. K., B. S. Lanchester, B. Gustavsson, N. Ivchenko, and H. Dahlgren (2010), Using multispectral optical observations to identify the acceleration mechanism respon-

sible for flickering aurora, *J. Geophys. Res., 115, A12315*, doi:10.1029/2010JA015805.

Whiter, D. K., B. S. Lanchester, B. Gustavsson, N. I. B. Jallo, O. Jokiaho, N. Ivchenko, and H. Dahlgren (2014), Relative brightness of the $O^+(^2D - ^2P)$ doublets in low-energy aurorae, *ApJ 797, 64*, doi:10.1088/0004–637X/797/1/64.

Yaegashi A, T. Sakanoi, R. Kataoka, K. Asamura, Y. Miyoshi, M. Sato, S. Okano (2011), Spatial-temporal characteristics of flickering aurora as seen by high-speed EMCCD imaging observations. *J. Geophys. Res., 116:A00K04*, doi:10.1029/2010JA016333.

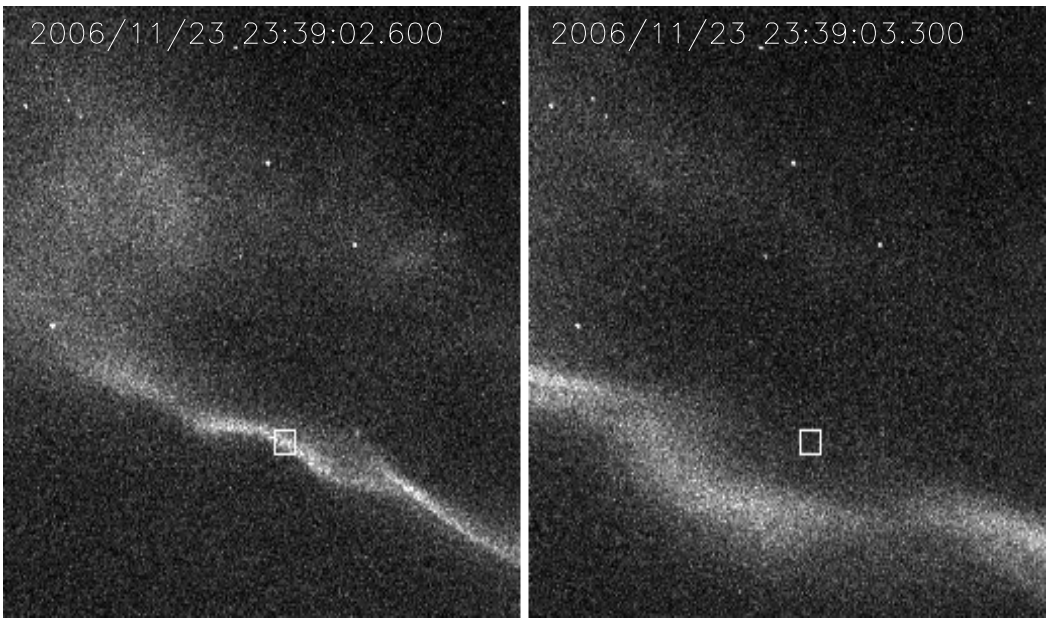

Figure 1. Left image shows a thin auroral filament observed in magnetic zenith (indicated with a white square) with a narrow FOV imager. The width of the structure is estimated to 80 m. Right image is the same filament 0.7 s later, as it has moved ∼1 km (at an assumed altitude of 100 km) from magnetic zenith. The 'width' is now estimated to be 600 m.

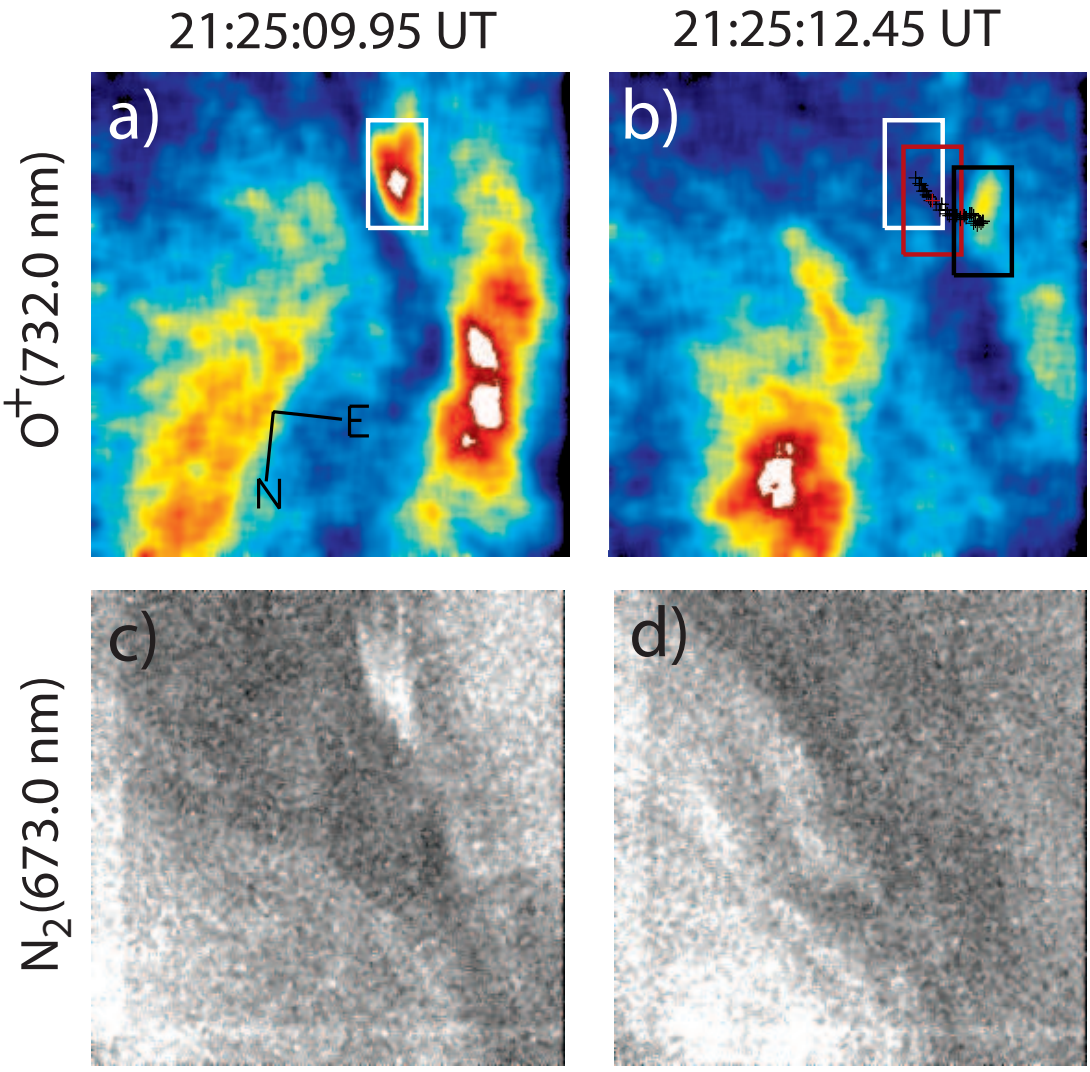

Figure 2. O^+ images from ASK at a) 21:25:09.95 UT and b) 21:25:12.45 UT. The motion of the afterglowing plasma within the box is traced using a cross-correlation method. The white boxes indicate the initial location of the plasma blob, black is the final location and red is its location as the prompt emission ceases. Prompt N_2 emissions at 673.0 nm are shown for comparison in c) and d) at these two instances of time.

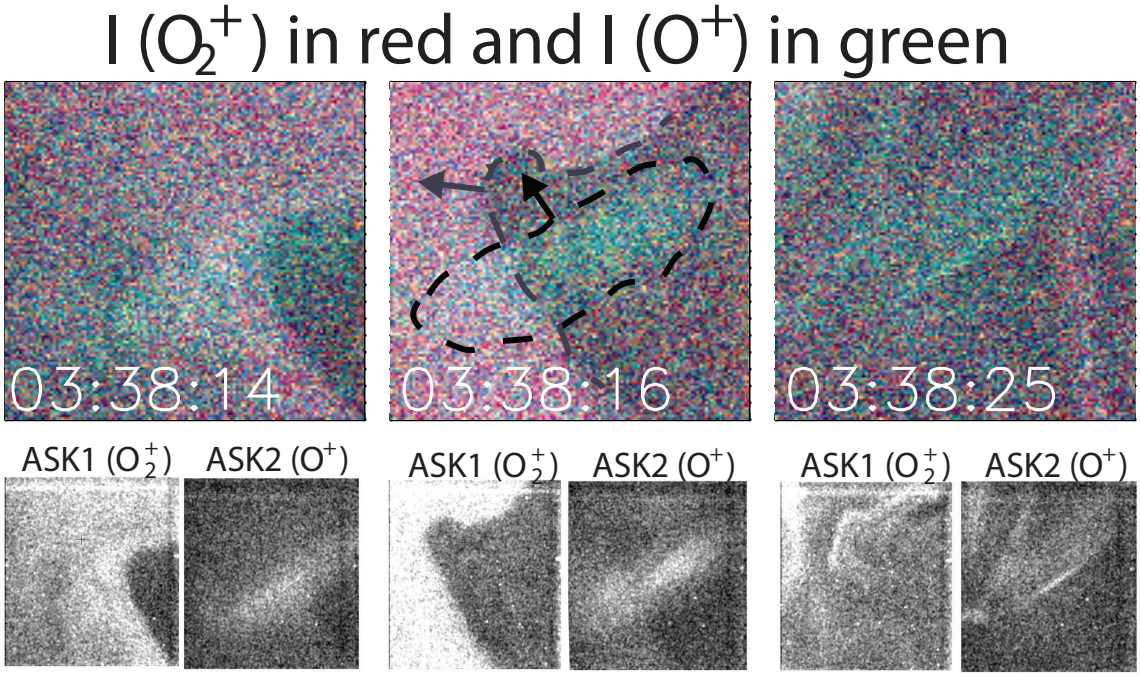

Figure 3. Top row: Overlaid simultaneous O_2^+ images (red) and O^+ images (green) show the temporal evolution of different structures caused by high energy precipitation (red features) and low energy precipitation (green features), respectively. The aurora takes different shapes in the O_2^+ image compared with the O^+ image. The edges of the features are marked in the middle panel, where the arrows indicate the direction of motion of the different, overlapping auroral structures. The bottom row shows the individual images from the two channels for each instant of time.